Hybrid functional study of hydrogen passivation in carbon-oxygen related defect complexes in silicon.

A. Abdurrazaq[a,b,*], W. E. Meyer[a]

[a] *Department of Physics, University of Pretoria, Pretoria 0002, South Africa.*
[b] *Ibrahim Shehu Shema Centre For Renewable Energy Research, Umaru Musa Yar'adua University, Dutsin-ma Road P.M.B. 2218 Katsina, Katsina State Nigeria.*

Abstract

Density functional theory (DFT) with the Heyd-Scuseria-Ernzerhof hybrid functional was used to predict the structure, formation energy, stability and the charge state transition energy levels induced by carbon-oxygen related complexes as a result of hydrogen passivation in silicon. Our results show that, in the neutral charge state the hydrogen interstitial (H_i) interacts with O_i, C_i, C_sO_i, C_iO_i, and C_sC_i to form a stable O_iH_i, C_iH_i, $C_sO_iH_i$, $C_iO_iH_i$, and $C_sC_iH_i$ defect complexes. Predicted charge state transition levels showed reasonable agreement with the experiment. The charge state transition energy levels were found to shift to the conduction band as a result of hydrogen passivation.

Keywords: Formation energy, Defect complexes, Charge states, Binding energy, Defect level

1. Introduction

Silicon is the most widely used material in sensor devices, microelectronics and photovoltaic applications. Despite our ability to manufacture high purity almost defect free silicon, defects in silicon still play a role either in as-grown material, or are produced during fabrication processes or exposure to radiation during use. As a result, a detailed understanding of the properties and the fundamental physics behind the behavior of defects in silicon is

*Corresponding author
**Corresponding author
Email address: a.abdurrazaq@up.ac.za (A. Abdurrazaq)

required in order to improve silicon devices as well as allow their use in new applications [1]. Carbon, oxygen and hydrogen are common impurity atoms found in silicon, and their presence is unavoidable [2]. Sometimes these impurities are intentionally introduced for example in solar cell fabrication of a front facing silicon nitride anti- reflection layer, which results in the reduction of surface recombination [3]. In order to understand the limitations in fabricating 'defect-free' silicon, as well as the behavior of defects in irradiated silicon, the study of carbon-oxygen-hydrogen related defect complexes is necessary [4, 5, 6, 7, 8, 9, 10, 11]. In Czochralski silicon, carbon normally occupies the substitutional position (C_s) and the oxygen interstitial (O_i) occupies the bond-center position [3]. Electron irradiation at low temprature generates silicon interstitials that displace C_s leading to the formation of C_i which is mobile and can react with an O_i to form the C_iO_i in high oxygen (CZ) material. A further C_i is able to displace the O_i to form C_sC_i defect complex in low oxygen float zone (FZ) material [12].

In the last few decades, the development of theoretical and computational hardware techniques have made it possible to model the electronic structure of point defects in semiconductors to an acceptable level of accuracy possible. Several atempts were made to model the carbon-oxygen-hydrogen related defect complexes, using the Generalised gradient approximation (GGA) and the Local density approximation (LDA). However the GGA and the LDA do not predict the band gap of semiconductors accurately, while the Heyd-Scuseria-Ernzerhof (HSE) functional is able to do so [13, 14]. Considering the fact that the charge state transition level is an important electrical property of a defect system, and approximetly corresponds to DLTS defect levels, we modelled some of the carbon-oxygen defect complexes together with the impact of hydrogen passivation on their formation energy, binding energy and the charge state transition energy levels using the HSE functional.

2. Computational Details

The plane wave density functional theory code QUANTUM ESPRESSO [15], and the HSE functional [16, 17], were used in this study. Norm-conserving pseudopotentials [18, 19] were employed to separate the valence electrons from the core electrons. The formation

energy of a vacancy in a 64-atom, 96-atom, and 128-atom silicon supercell using 45 Ry energy cutoff, and a $4 \times 4 \times 4$ Monkhorst-Pack [20] k-point mesh was found to be 4.01 eV, 3.99, ev and 3.98 eV. The difference between the 128-atom and 64-atom supercell is 0.03 eV. Then the total minimum energy of the 64-atom supercell was calculated using a $4 \times 4 \times 4$ Monkhorst-Pack [20] k-point mesh, with the energy cutoff varied from 10 Ry to 90 Ry at an interval of 5 Ry. The difference in the total minimum energy for both the neutral and the charged cell between the 40 Ry and the 45 Ry cutoff energy was found to be less than 0.1 meV per atom. The total minimum energy of the same supercell was also calculated using the 40 Ry energy cutoff, with the k-point mesh varied from $2 \times 2 \times 2$ to $8 \times 8 \times 8$ within the Monkhorst-Pack [20] scheme. The difference in the total minimum energy for both the neutral and the charged cell between the $3 \times 3 \times 3$ and the $8 \times 8 \times 8$ k-point was still found to be less than 0.1 meV per atom. Considering the fact that, HSE calculations is very expensive and that the difference in the formation energy between the 128-atom and 64-atom supercell is very small we decided to use the 64-atom silicon supercell with 40 Ry energy cutoff and $3 \times 3 \times 3$ k-point mesh for all the calculations. The structure was then optimised using HSE, and the band gap of silicon was calculated to be 1.18 eV which reasonably agrees with both theoretical and experimental predictions. [21, 22, 23]. The 64-atom supercell has previousely been used to model the properties of defects in Si [24, 25, 26]. The supercells containing the defects were then relaxed until the forces acting on each atom were less than 0.001 eV/Å and the difference in total energy between the iterations was less than 10^{-5} eV. The formation energy of a defect in a charge state q is derived from the energy of the supercell with the defect ($E(defect, q)$), the energy of the pristine supercell ($E(pristine)$), the chemical potential (μ_l) of the atoms introduced or removed, the energy of the valence band (E_V), the Fermi level (ε_F) and a correction term (E^q_{Cor}). This can be written as [27, 28, 29]

$$E^f(defect, q) = E(defect, q) - E(pristine) + \sum_l (\Delta n)_l \mu_l + q[E_v + \varepsilon_F] + E^q_{Cor}. \quad (1)$$

The electrostatic corrections E^q_{Cor} are computed using the Corrections For Formation Energy and Eigenvalues for charged defect simulations Package (CoFFEE) [30]. The dielectric

constant of silicon used in the correction approach was taken from ref [31]. The Fermi energy where the energies of formation of two charge states are equal is referred to as the charge state transition energy level and is given by [27]

$$\epsilon(q/q') = \frac{E^f(defect, q; \varepsilon_F = 0) - E^f(defect, q'; \varepsilon_F = 0)}{q' - q}. \quad (2)$$

The binding energy is the minimum energy required to dissociate a defect complex in to separate non-reacting defects. This is given by [29, 32]

$$E_b = \sum_l E^f_{isolated} - E^f_{defect-complex}. \quad (3)$$

Here $\sum_l E^f_{isolated}$ is the summation of the formation energies of the isolated defects, and $E^f_{defect-complex}$ is the formation energy of the defect complex.

3. Results and discussion

In this section, the geometric structure, formation energy, binding energy, and the thermodynamic charge transition levels of the O_i, C_i, C_sO_i, C_iO_i, C_iH_i, C_sC_i, O_iH_i, $C_sO_iH_i$, $C_iO_iH_i$, and $C_sC_iH_i$ are discussed.

3.1. Structural relaxation

Fig. 2 presents the structures of the defect complexes in the relaxed form and Table 1 presents the calculated shortest bond length distances in Å between silicon atoms and the introduced impurity atom. Defect complexes involving oxygen interstitials showed little relaxation. However, carbon interstitials relaxed significantly. The relaxed bond lengths of all the impurities with their nearest neighbour atoms were always shorter than the relaxed Si-Si bond length in the pristine environment. However, the carbon impurity at the substitutional site had the shortest relaxed bond length.

3.2. Formation energy

The energy of formation at neutral charge state of the O_i, C_i, C_sO_i, C_iO_i, and C_sC_i defect complexes together with the hydrogen passivated defect-complexes (O_iH_i, C_iH_i, $C_sO_iH_i$, $C_iO_iH_i$, and $C_sC_iH_i$) are displayed in Table 2. The chemical potential of oxygen was taken as zero in SiO_2 in order to avoid negative formation energies. The formation energy results showed that, the defect complexes could readily be formed in CZ silicon, where the concentration of oxygen and carbon impurities is significant.

3.3. Binding energy

In order to determine if the hydrogen passivated defect complexes can form, the binding energy for the respective defect complexes were calculated. The binding energy of the defect complexes in their neutral charge state are presented in Table 2. The feasibility of Si_i displacing C_s to form C_i was confirmed both for isolated C_s as well as the C_iO_i defect. While the binding energy results predict that H_i strongly bound with O_i and C_i to form the O_iH_i and C_iH_i defect complex. H_i could also be bound strongly to C_sO_i, C_iO_i and C_sC_i to form stable $C_sO_iH_i$, $C_iO_iH_i$ and $C_sC_iH_i$ defect complexes. C_sC_i had a low binding energy of 0.25 eV, while the binding energy of O_i in C_iO_i and C_sO_i was even lower at 0.19 eV and 0.09 eV respectively. This agrees with the experimental observation that C_sO_i is the first defect to be formed at low tempratures but very unstable whereafter, in silicon with high oxygen concentration, C_iO_i is formed and C_sC_i is formed in silicon with low oxygen concentration [12].

3.4. Thermodynamic charge state transition levels

The charge state transition energy levels (relative to the valence band) of the defect complexes relative to the valence band are presented in Table 3. We compared the defect levels with the available experimental data and previous DFT calculations. Fig. 1 presents the formation energy of the thermodynamically stable charge state of the defect as a function

of Fermi energy. Our results show that the oxygen interstitial (O_i) is an electrically inactive defect, which agrees with other theoretical predictions [7]. For O_iH_i, C_i, C_iH_i, C_iO_i and $C_sC_iH_i$, double donor level close to the valence band were theoretically predicted but not experimentally observed. In the case of C_iH_i, it might be close eneough to the valence band that could not be observed by DLTS. For the C_i and $C_sC_iH_i$ the other two donor levels predicted agreed with experiment while for the O_iH_i levels, two levels around E_V + 1.0 eV were predicted but only one observed experimentally. For the C_iO_i and $C_iO_iH_i$ only the donor level predicted in the lower half of the band gap was observed, while for the C_sC_i only the predicted acceptor level was observed, but the predicted acceptor level close to the valence band was not observed. Recently, Barnard *et al.* [33] observed defects believed to be the C_iH_i and $C_iO_iH_i$. In the case of the C_iH_i the experimental level agrees well with a predicted acceptor level. For the $C_iO_iH_i$, by ref [3] a level attributed to the $C_iO_iH_i$ agrees reasonably well with the predicted donor level, while the predicted acceptor level was observed by Barnard *et al.* [33]. The C_sO_i is probably too unstable to be observed. Except for O_i (which is electrically inactive) the theoretical calculations, the addition of H seems to have caused a shift of the charge transition levels to the conduction band by about 10-300 meV.

4. Summary

Hybrid density functional theory was used to investigate the formation energies, stability, and the thermodynamic transition energy levels of carbon-oxygen defect complexes before and after hydrogen passivation. The formation energies at zero charge state showed that H_i can readily interact with the carbon-oxygen complexes to form the carbon-oxygen-hydrogen defects complexes. The binding energies at zero charge state indicated that the defects are stable and do not dissociates before and after hydrogen passivation. The predicted charge state transition energy levels shift towards the conduction band of the defect energy levels after hydrogen passivation. Except for the predicted double donor levels which are not observed experimentally, the O_iH_i, C_i, C_sC_i, $C_iO_iH_i$, and $C_sC_iH_i$ showed good agreement with experimental DLTS levels. For C_iH_i, C_iO_i, one charge transition agreed well while the

other was not observed and for the $C_sO_iH_i$, some discrepancy between one predicted level and experiment was observed while the other predicted level agreed with experiment.

5. Acknowledgement

This work is based on the research supported partly by National Research foundation (NRF) of South Africa (Grant specific unique reference number (UID) 98961). The opinions, findings and conclusion expressed are those of the authors and the NRF accepts no liability whatsoever in this regard. The authors acknowledge the Center For High Performance Computing (CHPC) Cape Town, South Africa for computational resources.

References

[1] S.-R. Christopoulos, E. Sgourou, T. Angeletos, R. Vovk, A. Chroneos, C. Londos, Journal of Materials Science: Materials in Electronics 28 (14) (2017) 10295–10297.

[2] G. Kissinger, S. Pizzini, Silicon, germanium, and their alloys: growth, defects, impurities, and nanocrystals, CRC Press, 2014.

[3] J. Coutinho, R. Jones, P. Briddon, S. Öberg, L. Murin, V. Markevich, J. LindstrJöm, Physical Review B 65 (1) (2001) 014109.

[4] J. Coutinho, R. Jones, P. Briddon, S. Öberg, Physical Review B 62 (16) (2000) 10824.

[5] C. Londos, A. Andrianakis, V. Emtsev, H. Ohyama, Semiconductor Science and Technology 24 (7) (2009) 075002.

[6] A. Chroneos, C. Londos, E. Sgourou, P. Pochet, Applied Physics Letters 99 (24) (2011) 241901.

[7] H. Wang, A. Chroneos, C. Londos, E. Sgourou, U. Schwingenschlögl, Scientific reports 4 (2014) 4909.

[8] T. Angeletos, A. Chroneos, C. Londos, Journal of Applied Physics 119 (12) (2016) 125704.

[9] C. Londos, M. Potsidi, E. Stakakis, Physica B: Condensed Matter 340 (2003) 551–555.

[10] A. Chroneos, E. Sgourou, C. Londos, U. Schwingenschlögl, Applied Physics Reviews 2 (2) (2015) 021306.

[11] E. Sgourou, D. Timerkaeva, C. Londos, D. Aliprantis, A. Chroneos, D. Caliste, P. Pochet, Journal of Applied Physics 113 (11) (2013) 113506.

[12] L. Song, X. Zhan, B. Benson, G. Watkins, Physical Review B 42 (9) (1990) 5765.

[13] P. Deak, B. Aradi, T. Frauenheim, E. Janzen, A. Gali, Physical Review B 81 (15) (2010) 153203.

[14] J. Kusima, J. Ojanen, J. Enkovara, T. Rantala, Physical Review B 82 (11) (2010) 115106.

[15] P. Giannozzi, S. Baroni, N. Bonini, M. Calandra, R. Car, C. Cavazzoni, D. Ceresoli, G. L. Chiarotti, M. Cococcioni, I. Dabo, et al., Journal of physics: Condensed matter 21 (39) (2009) 395502.

[16] J. Heyd, G. E. Scuseria, M. Ernzerhof, The Journal of chemical physics 118 (18) (2003) 8207–8215.

[17] A. V. Krukau, O. A. Vydrov, A. F. Izmaylov, G. E. Scuseria, The Journal of chemical physics 125 (22) (2006) 224106.

[18] C. Hartwigsen, S. Gœdecker, J. Hutter, Physical Review B 58 (7) (1998) 3641.

[19] S. Goedecker, M. Teter, J. Hutter, Physical Review B 54 (3) (1996) 1703.

[20] H. Monkhorst, J. Pack, Physical Review B 13 (1976) 5188.

[21] J. Heyd, J. E. Peralta, G. E. Scuseria, R. L. Martin, The Journal of chemical physics 123 (17) (2005) 174101.

[22] J. Paier, M. Marsman, K. Hummer, G. Kresse, I. C. Gerber, J. G. Ángyán, The Journal of chemical physics 124 (15) (2006) 154709.

[23] P. Haas, F. Tran, P. Blaha, Physical Review B 79 (20) (2009) 209902.

[24] H. Wang, A. Chroneos, C. Londos, E. Sgourou, U. Schwingenschlögl, Applied Physics Letters 103 (5) (2013) 052101.

[25] S.-R. Christopoulos, H. Wang, A. Chroneos, C. A. Londos, E. N. Sgourou, U. Schwingenschlögl, Journal of Materials Science: Materials in Electronics 26 (3) (2015) 1568–1571.

[26] H. Wang, A. Chroneos, D. Hall, E. Sgourou, U. Schwingenschlögl, Journal of Materials Chemistry A 1 (37) (2013) 11384–11388.

[27] C. Freysoldt, B. Grabowski, T. Hickel, J. Neugebauer, G. Kresse, A. Janotti, C. G. Van de Walle, Reviews of modern physics 86 (1) (2014) 253.

[28] Y. Kumagai, F. Oba, Physical Review B 89 (19) (2014) 195205.

[29] G. Zollo, Y. Lee, R. Nieminen, Journal of Physics: Condensed Matter 16 (49) (2004) 8991.

[30] M. H. Naik, M. Jain, Computer Physics Communications 226 (2018) 114–126.

[31] J. Paier, M. Marsman, G. Kresse, Physical Review B 78 (12) (2008) 121201.

[32] E. Igumbor, R. C. Andrew, W. E. Meyer, Journal of Electronic Materials 46 (2) (2017) 1022–1029.

[33] A. Barnard, W. E. Meyer, F. D. Auret, V. Kolkovosky, Physica B to be Submitted.

[34] K. Bonde, L. Dobaczewski, S. Sogard, B. Bech, Physical Review B 65 (2002) 075205.

[35] P. Mooney, L. Cheng, M. Süli, J. Gerson, J. Corbett, Physical Review B 15 (8) (1977) 3836.

[36] L. Kimerling, Inst. Phys. Ser. 31 (1977) 221.

[37] L. Song, G. Watkins, Physical Review B 42 (9) (1990) 5759.

[38] O. Andersen, A. R. Peaker, L. Dobaczewski, K. Bonde, B. Hourahine, R. Jones, P. Briddon, s. öberg, Physical Review B 66 (1) (2002) 235205.

[39] R. Stubner, V. Kolkovsky, J. Weber, Applied Physics Letters 118 (2016) 055704.

[40] C. N. Ouma, W. E. Meyer, Computational Materials Science 118 (2016) 338–341.

[41] A. L. S. Ferreira-Resende, Phd Thesis 31 (2000) 31054863.

Table 1: Predicted bond length and bond angle, between the impurity atoms and the nearest Si atom after relaxation of the neutral defect. The bond length α_d is before relaxation, (with atoms placed at high symmetry points) β_d is after relaxation and Δ_d is the absolute difference between the bond lengths before and after relaxation and θ is the bond angle between the impurity atom and the next nearest neigbor silicon atom. All values of bond length are in Å and bond angle θ in degrees

Bonds	α_d	β_d	Δ_d	θ
O-Si	1.71	1.79	0.08	115.02
C-Si (C_i)	2.03	1.93	−0.10	93.10
C-Si (C_s)	2.37	2.20	−0.17	102.91
H-Si	2.03	1.88	−0.15	70.52

Table 2: The formation energy E^f at $\varepsilon_F = 0$, and binding energy B_E of the above defects in eV

Defect	Reaction	B_E=− Δ E^f	E^f
O_i	−	−	2.14
O_iH_i	O_i + H_i	0.49	3.52
C_i	−	−	1.07
C_iH_i	C_i + H_i	0.62	2.33
C_sO_i	C_s + O_i	0.09	2.40
$C_sO_iH_i$	C_sO_i + H_i	0.69	3.58
C_iO_i	C_i + O_i	0.19	3.02
C_i	C_s + Si_i	0.97	1.07
C_iO_i	C_sO_i + Si_i	2.75	3.02
$C_iO_iH_i$	C_iO_i + H_i	0.91	3.98
C_sC_i	C_s + C_i	0.25	1.17
$C_sC_iH_i$	C_sC_i + H_i	0.40	2.64

Table 3: The thermodynamic charge state transition energy levels $\epsilon(q/q')$ in eV with respect to the energy of the valence band E_V for the defects considered in this study

Defect	Reference	$(+2/+1)$	$(+1/0)$	$(0/-1)$
O_i	This study	Inactive.		
	Theory [7]	Inactive.		
O_iH_i	This study	0.23	0.96	1.10
	Experimental [34]	–	1.00	–
C_i	This study	0.27	0.30	1.04
	Experimental [35, 36], [37]	–	0.28	1.06
C_iH_i	This study	0.05	0.32	1.07
	Experimental [33]	–	–	1.03(?)
C_sO_i	This study	–	0.67	–
$C_sO_iH_i$	This study	–	1.00	1.14
	Experimental [38, 39]	–	0.33	1.01
C_iO_i	This study	0.17	0.40	0.71
	Experimental [35]	–	0.38	–
$C_iO_iH_i$	This study	–	0.50	0.78
	Experimental [3]	–	0.41	–
	Experimental [33]	–	–	1.08(?)
C_sC_i	This study	–	0.02	0.78
	Theoretical [40]	–	0.06	0.79
	Experimental [12]	–	–	1.00
$C_sC_iH_i$	This study	0.18	0.33	1.00
	Experimental [41]	–	0.38	0.97

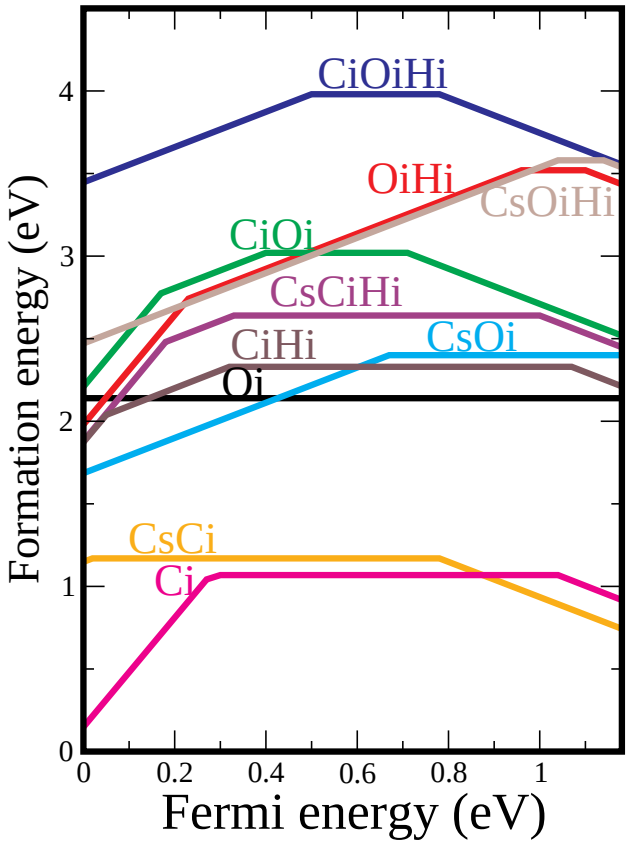

(a)

Figure 1: The thermodynamic accessible charge states for O_i, O_iH_i, C_sO_i, $C_sO_iH_i$, C_iO_i, $C_iO_iH_i$, C_sC_i and $C_sC_iH_i$ defect complexes. The formation energy scale ranges from 0 to 5 eV and the Fermi energy scale ranges from 0 to 1.18 eV.

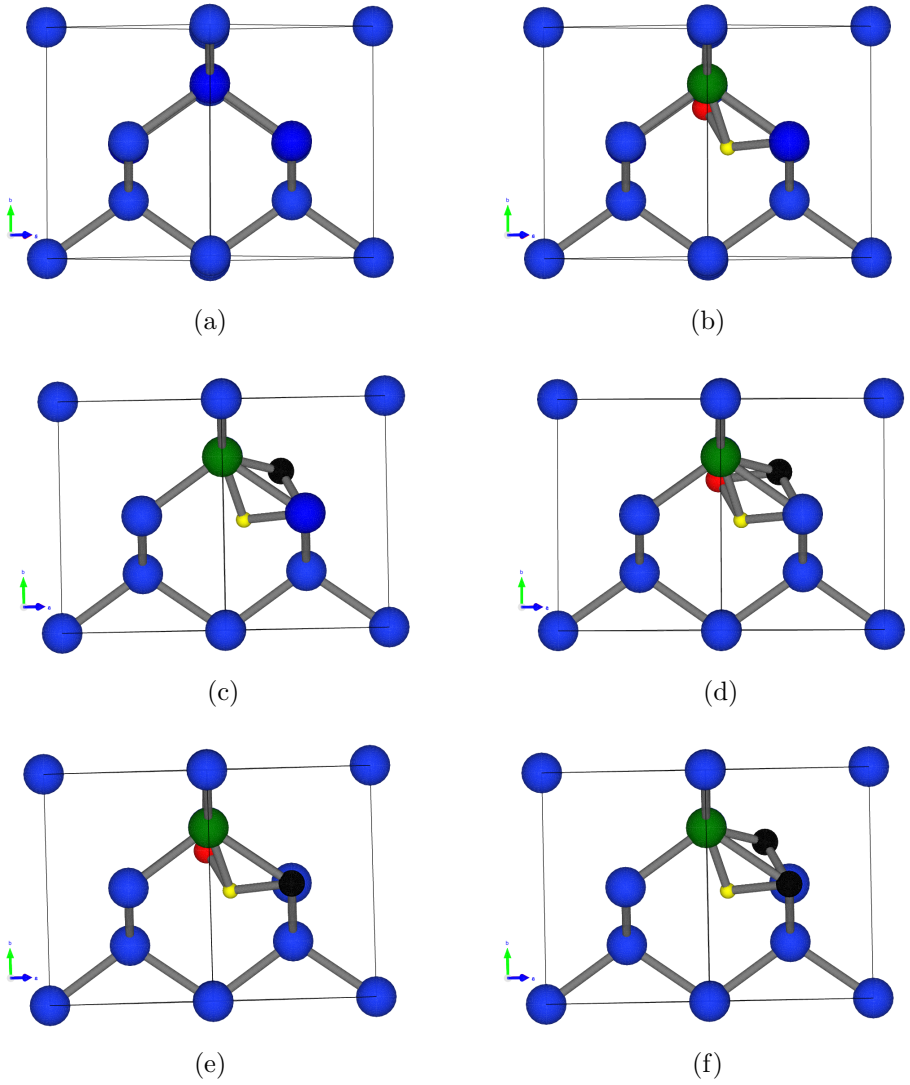

Figure 2: The relaxed geometric structures of the (a) pristine, (b) O_iH_i, (c) C_iH_i (d) $C_iO_iH_i$, (e) $C_sO_iH_i$, and (f) $C_sC_iH_i$. The blue balls represents silicon atoms, the green ball represent the next nearest neigbor silicon atom with respect to all the defects, the black balls represents carbon atom, the red balls represent oxygen atom and the yellow balls represent hydrogen atoms repectively.